MODIFICATION OF SURFACE WETTABILITY OF SODIUM IONOMER SHEETS VIA ATMOSPHERIC PLASMA TREATMENT

J.M. España, D. García, L. Sánchez, J. López, R. Balart.

Materials Technology Institute

Universidad Politécnica de Valencia (Alcoy campus)

Plaza Ferrandiz y Carbonell, 1 03801 Alcoy (Alicante)

ABSTRACT

In this study atmospheric plasma treatment has been used to modify the wetting properties of ethylene-methacrylic acid sodium ionomer. The effects of the plasma treatment on surface properties of this ionomer have been followed by contact angle measurements, Fourier transformed infrared spectroscopy (FTIR), scanning electron microscopy (SEM) and atomic force microscopy (AFM). With the use of these techniques, the overall effects on activation-functionalization and surface topography changes have been determined in terms of the processing parameters of the atmospheric plasma treatment (rate and distance). The obtained results show a remarkable increase of the wetting properties and optimum balanced behaviour is obtained for atmospheric plasma treatment with a rate of 100mm·s^{-1} and a distance of 6mm; in this case, surface free energy is increased from 33 mJ m^{-2} (untreated ionomer) up to 62 mJ m^{-2}, maintaining good transparency.

INTRODUCTION

The surface chemical properties of solid substrates affect their behaviour in industrial applications. A number of techniques can be used to modify substrate surfaces (abrasion, photoactivators and chemical agents, to name a few) but in recent years research has focused on processes that can change substrate surfaces without altering the general properties of the solids themselves (heat or electrical treatments). Plasma-based techniques have attracted the most interest from the industrial standpoint, as they are able to change the surface properties of solids rapidly and cleanly without generating any residue. Moreover, plasma technology can be easily adapted to materials processing at the industrial level [1-6].

Polymer materials are quite attractive to industry, a sector which constantly demands new materials for special applications requiring versatility in design, density, cost and other properties such as ease of processing. This family of materials includes ionomers, which are copolymers whose structure contains ionic charges (generally from lithium, sodium or magnesium). These ionic charges in the copolymer cause it to behave differently during crystallization, resulting in low fusion and softening points. This characteristic gives the material excellent optical properties, which are the result of lower crystallinity, giving the polymer greater transparency and clarity. These ionomers also have optimal mechanical properties, with great flexibility and durability [7, 8]. They can also be processed more easily, via processing methods such as extrusion and injection moulding, which are used in the manufacture of thermoplastics. Yet a significant drawback of this material in terms of technological demands is its low adhesion when bonded with other materials or used with primers. This poor adhesion is

due to the ethylene found in its structure. This is why the surface of these materials usually requires prior treatment before being used.

The principal methods employed to improve the ionomer's hydrophobic behaviour (a result of its low polarity) are based on modification of the material's surface [9]. The sodium ionomer used in this study possesses low surface energy (around 33 mJ·m^{-2}), which hinders the adhesion process during processing. From the industrial standpoint, one of the more interesting surface treatments that can be used to improve the surface properties of the ionomer is treatment by atmospheric plasma. Polymers treated with this type of plasma have shown increased wettability, owing to the action of the plasma which modifies surface functionality, thereby increasing surface energy (γ_s), providing the polymer with hydrophilic properties [10-14]. This effect is the result of the formation of free radicals over the surface of the treated ionomer; an interaction occurs between the ionomer chains and the ionized species created by the plasma current and from reactions with the air. Once the ionomer is treated, its surface is activated due to the presence of various polar groups containing oxygen (esther, alchohol, ketone, peroxide and carboxylic acid, among others). These free radicals that have formed on the treated surface of the ionomer react with the species in the atmosphere and chemically modify the surface and as a consequence its initial hydrophobic behaviour. This process improves the material's wettability (for adhesion or printing) [10, 15, 16].

Some authors have evaluated the effects of plasma treatments on the wettability of the treated substrate surfaces using the contact angle measuring technique [17, 18]

and have observed the formation of chemical species on the surface of the substrate using the FTIR spectroscopy [19, 20].

In this study we used the atmospheric plasma technique to modify wettability of an ionomer sheet; the ionomer was an ethylene-methacrylic acid copolymer characterised by a sodium ion (Na^+) aggregate structure. The effects of this surface treatment on ionomer sheets were quantified using contact angle measurements, Fourier transform infrared spectroscopy (FTIR-ATR), scanning electronic microscope (SEM) and atomic force microscopy (AFM) to identify changes to the surface of the ionomer samples. The authors also determined which process parameters influence the uniformity and homogeneity of the treated surface.

EXPERIMENTAL

Materials

An ethylene-methacrylic acid copolymer based sodium ionomer commercial grade Surlyn PC-100 (DuPont, Barcelona, Spain) in pellet form, suitable for injection molding, has been used in this work as a base substrate for surface modification by atmospheric plasma. It is characterized by a melt flow index (190 ºC and 2.16 kg) of 1.09 g/10 min.

Ionomer sheets sizing 160x60x2 mm were obtained by conventional injection molding process in a Mateu-Solé, mod. 270/5 (Mateu-Solé S.A. Barcelona, Spain).

Four different test liquids for contact angle measurements were selected to provide a wide range of dispersive and polar constant values: diiodomethane 99% stabilized supplied by Acros (Acros Organics, Geel, Belgium), formamide ACS and glycerol 99% extra pure supplied by Scharlau (Scharclau Chemie S.A, Barcelona,

Spain), and double distilled water. Table 1 shows the polar and dispersive components of the different test liquids selected for appropriate surface free energy calculation.

TABLE 1

Air atmospheric plasma treatment

Injection molded sheets were subjected to air atmospheric plasma treatment in a Plasmatreat FG 3001 (Plasmatreat GmbH, Steinhagen, Germany) plasma reactor. The plasma generator operates at 50/60 Hz, 230 V and 16 A and is equipped with a rotational nozzle. This equipment works by injecting compressed air at a pressure of 2 bars.

Different nozzle/substrate in the 6-20 mm range and different rates in the 100-1000 mm s^{-1} were selected to evaluate the effects of the processing parameters of the atmospheric plasma treatment on wetting properties of ionomer substrates.

Contact angle measurements and surface free energy calculation

Contac angle measurements were done with an optical goniometer EasyDrop Standard mod. FM140 110/220 V, 50/60 Hz (Krüss GmbH, Hamburg, Germany). The goniometer is equipped with the software Drop Shape Analysis SW21 for quantitative evaluation of wettability. Measurements of contact angles were carried out 5 min after the plasma treatment for all samples and the maximum error did not exceed ±3%.

The Owens-Wendt method was selected to calculate surface free energy values of the plasma-treated ionomer samples. This method is useful since it takes into account the polar (γ_s^p) and dispersive (γ_s^d) contributions to the total surface free energy (γ_s). The

use of different test liquids with different polar (γ_l^p) and dispersive (γ_l^d) components allows accurate estimation of the solid surface free energy.

$$\gamma_l \cdot (1+\cos(\theta))/2(\gamma_l^d)^{1/2} = (\gamma_s^p)^{1/2} \cdot \left[\left(\gamma_l^p \right)^{1/2} / \left(\gamma_l^d \right)^{1/2} \right] + \left(\gamma_s^d \right)^{1/2} \qquad \text{(eq. 1)}$$

Where θ is the measured contact angle, γ_l is the liquid surface tension, γ_s is the solid surface free energy of the substrate. The superscripts "p" and "d" refer to the polar and dispersive contributions respectively. From the observation of equation 1, it is evident that a plot representation of $\gamma_l \cdot (1+\cos(\theta))/2 \, (\gamma_l^d)^{1/2}$ versus $(\gamma_l^p)^{1/2}/(\gamma_l^d)^{1/2}$ for the different tests liquids and the corresponding contact angle values, leads to a linear adjust (y=a+bx) in which, the slope represents $(\gamma_s^p)^{1/2}$ and the intercept is $(\gamma_s^p)^{1/2}$, so that it is possible to obtain the total surface free energy as the sum of the polar and dispersive contributions, $\gamma_s = \gamma_s^p + \gamma_s^d$.

Surface characterization

Chemical changes produced by the atmospheric plasma treatment were followed by Fourier transformed infrared spectroscopy (FTIR) with a Perkin Elmer, mod. FTIR Spectrum BX (Perkin Elmer, Massachusetts, USA) equipped with an Attenuated Total Reflectance (ATR) accessory mod. MIRacle (Pike Technologies, Madison, USA). Each sample was subjected to 10 scans from 4000 to 800 cm^{-1}, and the final spectrum is the average of them, spectra were scanned with a step of 2 cm^{-1} and a resolution of 4 cm^{-1}.

Qualitative observation of surface morphology of plasma-treated ionomer sheets was analyzed with a scanning electron microscope (SEM) supplied by FEI, mod. Phenom (FEI Company, Eindhoven, The Netherlands) with an applied voltage of 5 kV. Prior to each measurement, samples were subjected to a sputtering process with a

platinum-aurum allow with a sputter coater model SC7620 (Quorum Technologies, Kent, UK).

Quantitative characterization of surface topography of plasma-treated sheets was carried out with a atomic force microscope (AFM) Multimode with a constant force of 42 N m^{-1} and a resonance frequency of 320 Hz equipped with a Nanoscope IIIa ADCS controller (Veeco Metrology Group, Cambridge, United Kingdom).

Results and Discussion

Influence of atmospheric plasma conditions on surface wettability

The action of the atmospheric plasma on the ionomer sheets under consideration results in the functionalisation of the sheets' surface, due to the interaction of the ionized species from the air that are generated by the plasma. This increases the wettability of the ionomer samples. This increase, however, depends greatly on the processing variables of the atmospheric plasma during its application to the surface. This factor must be borne in mind when processing to optimise atmospheric plasma parameters (scan velocity and nozzle-substrate distance). This can be done by analysing the variation in contact angles which indicates the extent to which the surface is hydrophilic or hydrophobic.

Tables 2, 3, 4 and 5 show values for contact angles on the ionomer sheets treated with atmospheric plasma at various nozzle-substrate distances and at various scanning speeds using different contact liquids. The different contact liquids allow us to study changes in wettability of ionomer sheets as a function of application conditions in the plasma treatment.

TABLE 2, TABLE 3, TABLE 4 and TABLE 5

It is important to bear in mind that untreated ionomer sheets are hydrophobic, given the high values found in contact angles from the four different contact liquids used (Table 6).

TABLE 6

Analysis of the data contained in the above tables shows that in general, for any nozzle-substrate distance, contact angles decrease in value as treatment velocity increases, reaching a minimum value at a low velocity. Similarly, comparison of the results observed for every nozzle-substrate distance at a fixed velocity revealed that as nozzle-substrate distance increases, so does the contact angle, resulting in lower wettability. This observation is confirmed when different water contact angles for each nozzle-substrate distance were compared with contact angle measurements for the untreated sample fixed at the minimum velocity; it was found that at a distance of 6 mm there was a 68.3 % decrease in the contact angle, at a distance of 10 mm there was a 44.5% decrease, at a distance of 14 mm the contact angle decreases by 23.8% and at a distance of 20 mm, there is a 22.5% decrease in the contact angle.

Surface energy of the various treated samples was calculated by applying the Owens-Wendt method to the contact angle values. The figures below show the variation in surface energy (γ_s), variation in the polar component of the surface energy (γ_s^P) and

the variation in the dispersive component of the surface energy ($\gamma_s{}^d$), as a function of treatment velocity for each nozzle-substrate distance.

FIGURE 1

Figure 1 shows the change in surface energy as a function of plasma treatment velocity, at a distance of 6 mm between nozzle and substrate. Under these processing conditions, the ionomer shows an 180% increase in surface energy with respect to the untreated sample under low plasma application velocities (100 and 300 mm/s), with its surface energy increasing from 33.2 mJ·m^{-2} to 62.15 mJ·m^{-2}. This increase is shown in the graph: treatment velocity influences the plasma treatment which shows a decrease of 61.20% between the sample treated at 100 mm/s and the sample treated at 1000 mm/s, its surface energy decreasing from 62.15 mJ·m^{-2} to 38.05 mJ·m^{-2}.

The change in the polar component ($\gamma_S{}^P$) of the surface energy is identical to that of the total surface energy (γ_S). The untreated sample showed low values of the order of 8.05 mJ·m^{-2}, which improved under low treatment velocities, reaching a value of 34.85 mJ·m^{-2} at 100 mm/s. As treatment velocities increased, however, these values decreased to 15.13 mJ·m^{-2} at 1000 mm/s. In contrast, the dispersive component ($\gamma_S{}^d$) of the surface energy varied slightly, increasing by 11% over its initial value, reaching a maximum value at a velocity of 300 mm/s. As velocity was increased, however, the surface energy decreased by 18% of the maximum value at a speed of 1000 mm/s.

FIGURE 2

Figure 2 shows the change in surface energy (γ_S), as well as its polar (γ_S^P) and dispersive components (γ_S^d), as a function of the atmospheric plasma treatment velocity at a nozzle-substrate distance of 10 mm. Samples treated at this distance show results that are similar to those treated at a distance of 6 mm. Although the distance between the nozzle and the substrate has been increased, the effect produced by the plasma on the surface of the ionomer sheet shows similar variations in surface energy. Surface energy (γ_S) increases at lower treatment velocities, showing a 159% increase. As said velocity increases, however, the surface energy at maximum treatment velocity decreases by about 30% of its maximum value. The behaviour of the polar component (γ_S^P) of the surface energy is the same as that of total surface energy; its value increases at low velocities and decreases as treatment velocity increases. The dispersive component (γ_S^d), however, remains nearly constant, showing an increase of just 4% at low treatment velocities with respect to the untreated sample values, and decreases by 12% with respect to its maximum value at high plasma treatment velocities.

FIGURE 3

The change in surface energy (γ_S) and its polar (γ_S^P) and dispersive components (γ_S^d) for a nozzle-substrate distance of 14 mm is shown in Figure 3. Here we observe that the behaviour of surface energy and its components is similar; they all attain a maximum value at low treatment velocity (100 mm/s). Surface energy increases by 142% with its polar component increasing by 199% and its dispersive energy increasing by 123%. As plasma treatment velocity increases, surface energy decreases as does its component energies.

FIGURE 4

Figure 4 shows the values for surface energy and its polar (γ_S^P) and dispersive (γ_S^d) components for samples treated at a nozzle-substrate distance of 20 mm. These treatment conditions are the least conducive to surface modification as they result in only minor variations in surface energy. As in the previous cases, maximum surface energy is achieved at low plasma treatment velocities (100 mm/s), resulting in an increase of 134% for surface energy, 175% for the surface energy's polar component and 121% for its dispersive component. As was observed in previous treatments, as plasma treatment velocity increases, the effectiveness of the treatment decreases, thereby decreasing the surface energy of the samples.

Surface Morphology

Surface modification of the sodium ionomer sheets treated with atmospheric plasma under different conditions was analysed using an atomic force microscope (AFM) in order to examine the surface roughness of the ionomer samples [25-27].

The morphology of the original untreated sample was found to be quite regular and homogeneous, whereas the sample treated with plasma at a nozzle-substrate distance of 6 mm showed an increased roughness that featured deeper grooves. Examination of this roughness revealed the presence of microetching. Etching is one of the ways in which the plasma treatment acts upon the material; during this process the surface of the material is bombarded with plasma. This action causes the values of the

dispersive component (γ_S^d) of the surface energy to increase, thereby increasing the hydrophilic nature of the ionomer surface [28-31].

As the nozzle-substrate distance increases, this microetching effect decreases, as can be observed in Figure 5.

FIGURE 5

In Figure 5 we see how abrasion or microetching density decreases in samples as nozzle-substrate distance is increased. At greater distances, the atmospheric plasma treatment is less effective, thereby lessening surface roughness. Roughness is lowest at a distance of 20 mm, as greater distances lessen the ability of the plasma to etch the ionomer surface, owing to lower plasma strength at this distance when compared to shorter distances.

A similar effect occurs as samples are passed under the plasma beam at higher velocities; surface abrasion decreases since its effect on the ionomer surface is weaker. Therefore the abrasion effect will be accentuated at lower scan velocities whereas high velocities do not bring about great differences in the surface morphology of the samples.

To examine the extent of microetching on the surface of the samples treated with atmospheric plasma an atomic force microscope (AFM) was used. Figure 6 shows the change in roughness of profiles for samples treated at a nozzle-substrate distance of 6 mm at various scan velocities.

FIGURE 6

Figure 6 shows that untreated samples were found to have a fairly homogeneous and regular profile, free of any pronounced roughness. As was observed previously with regard to the effect of the scan velocity of the sample, as said plasma scan velocity increases, the roughness decreases. This was confirmed in the above graph which shows the evolution of sample profiles indicating that at a low velocity (100 mm/s) the sample was found to have marked peaks and irregularities (in the form of level changes and grooves) which clearly indicate that the plasma's abrasive effect was greater. As the plasma scan velocity increases, peaks soften and grooves created by the abrasive action of the plasma decrease in depth.

FIGURE 7

The same effect was observed at a plasma application distance of 10 mm. The highest degree of surface roughness was observed at the lowest scan velocity (100 mm/s), and, as in the previous case, higher velocities lessen the strength of the treatment as well as surface roughness. A similar result was observed at nozzle-substrate distances of 14 and 20 mm (Figures 8 and 9 respectively). As was observed and discussed for Figure 5, the resulting roughness for these two distances decreases for samples treated at velocities greater than the 100 mm/s, as this velocity gives rise to the greatest surface roughness.

FIGURE 8 and FIGURE 9

TABLE 7

Table 7 shows the mean roughness parameters (Rms) and maximum roughness (Rmax) obtained from the AFM analysis. The roughness of untreated sample was low when compared to that of treated samples, which showed a considerable increase in roughness. This is attributable to the effect of microetching created by the plasma on the surface of the samples. As this microetching effect decreases with increasing velocity and distance, roughness too will decrease. The increase in surface roughness significantly increases wetting characteristics of the material. The results obtained by way of AFM analysis contrast with results obtained in the wettability study and the calculation of surface energy performed previously.

Characterisation of plasma activated surface

To study chemical changes produced by the atmospheric plasma process the surface was analysed by way of FTIR-ATIR. The action of the plasma produces oxidation of the surface species of the sample which increase its polarity; however, in this case the ionomer sample already contains some oxygen and therefore new chemical species are not created. Instead the quantity of compounds containing oxygen will increase resulting in an increase in the peaks associated with said compounds as was observed in Figure 10 [29, 32].

FIGURE 10

The peaks found in both the control and plasma-treated samples that are most relevant to our analysis are as follows: From left to right, located between 2916 and 2847 cm^{-1}, are peaks which indicate the presence of –CH$_3$ and –CH$_2$ groups (polyoefins). The peak located at 1698.55 cm^{-1} is characteristic of the C=O group which is present in carboxylic acids and originate in methacrylic acid found in the ionomer. Between 1560 and 1542 cm^{-1} there appear a series of peaks of the COO- group (Carboxylic acids). In this instance as in the previous case this compound comes from methacrylic acid of the sample. The peaks at 1465.89 and 1370.80 cm^{-1} correspond to the CH$_3$ group which is characteristic of polyoefins, similar to the first groups mentioned above. The remaining peaks at 1401.15 cm^{-1}, (–OH group), 1259.53 cm^{-1}, (C-O-C group), and 717.34 cm^{-1}, (O-C=O group) correspond to the various bonds associated to carboxylic acid molecules [33, 34].

After plasma treatment, the peaks that undergo slight variations are those containing oxygen in their functional group, due to the oxidising effect of the plasma. Of these, the peak that undergoes the greatest change as a function of the velocity of the treatment and plasma application distance is the peak at 1698.55 cm^{-1}.

TABLE 8

Table 8 lists the values for the area under peak 1689.55 cm^{-1}, for the different plasma treatment distances. Although these values show slight differences, this peak was the only one where a significant change was observed in area unit values. A minimum area was observed for the untreated ionomer sample, whereas the maximum peak area was seen for the minimum nozzle-substrate distance of 6 mm. As the nozzle-

substrate distance increases, the values for this area decrease. This can be explained by the oxidising action of the plasma which decreases in strength as the distance between the sample and the nozzle increases.

In order to study oxidative action as a function of scan velocity, scan velocity was varied for each nozzle-substrate distance. In this instance, only a slight variation was found at peak 1698.55 cm^{-1}.

The following tables list area values for peak 1698.55 cm^{-1} for the different plasma treatment distances.

TABLE 9, TABLE 10, TABLE 11 and TABLE 12

Analysis of the values shown in these tables revealed a similar pattern for all groups of results, where the maximum value for area is seen at the lowest velocity applied (100 mm/s). As velocity of plasma treatment increases, however, the area values decrease. This occurs because at low velocities, the action of the plasma is stronger; when the sample is passed under the plasma slowly, there is more time for the plasma beam to act on the surface. At higher velocities the sample passes under the plasma so rapidly that the plasma has very little time to have an oxidising effect on the surface, unlike the effect seen at lower velocities.

Conclusions

The following conclusions can be made regarding the atmospheric plasma processing conditions and their influence on surface wettability: With regard to the effect of the plasma, that is, both its oxidising action on the surface and the phenomenon of microetching, we observed that changes to sample sodium ionomer surfaces were greater at shorter nozzle-substrate distances, bringing about a greater wettability of the surface and greater surface energy. Similarly, plasma application velocity was found to have an affect on plasma action; at lower application velocities surfaces underwent greater changes than at higher velocities. Wettability and surface energy increased at lower velocities but decreased as plasma scan velocity increased.

With regard to surface morphology of the samples, as seen above, samples analysed by way of atomic force microscopy (AFM) showed greater surface roughness with decreasing nozzle/substrate distance with roughness decreasing as said distance increased. At low plasma application velocities the highest values of surface roughness were observed; as plasma scan velocity was increased surface roughness decreased.

Analysis of the plasma activated surface via FTIR-ATR revealed an increase in functional groups containing oxygen, especially the C=O group represented by the peak at 1698.55 cm^{-1} which corresponds to carboxylic acid, its presence attributable to the oxidising action of the plasma. At a fixed scan plasma velocity and varying nozzle-substrate distances, the shortest distance of 6 mm shows a maximum area for this peak associated to the C=O group of the sample. As the nozzle-substrate distance increases, however, this area decreases, which indicates lower quantities of said group. At a fixed nozzle-substrate distance with varying plasma application velocities, there is a maximum peak area for the C=O functional group at low velocities (100 mm·s^{-1}). As

scan velocity increases, however, this area decreases, which means that at lower velocities there is a greater presence of the carboxylic acid C=O group and as velocity increases, this group decreases. This occurs because when scan velocity increases, the plasma has less time to act upon the surface of the sample. Therefore as treatment time decreases, so does the effectiveness of the treatment.

Acknowledgements

References

1. T. Hassel, C. Birr, and F.W. Bach, *Coatings in Manufacturing Engineering*. **438**, (2010).

2. S.M. Hosseini, S.S. Madaeni, A.R. Khodabakhshi, and A. Zendehnam, *Journal of Membrane Science*. **365**, 1-2, (2010).

3. L.C. Kumruoglu and A. Ozel, *Materials and Manufacturing Processes*. **25**, 9, (2010).

4. Y. Kusano, S.V. Singh, A. Bardenshtein, N. Krebs, and N. Rozlosnik, *Journal of Adhesion Science and Technology*. **24**, 11-12, (2010).

5. C. Loghin, M. Ursache, R. Muresan, and A. Muresan, *Industria Textila*. **61**, 6, (2010).

6. W. Tillmann, E. Vogli, and S. Momeni, *Advanced Engineering Materials*. **12**, 11, (2010).

7. Z. Fang, S.F. Wang, S.Q. Wang, and J.P. Kennedy, *Journal of Applied Polymer Science*. **88**, 6, (2003).

8. R.M. Gohil, *Polymer Engineering and Science*. **49**, 3, (2009).

9. K. Suchocka-Galas and J. Kowalonek, *Surface Science*. **600**, 5, (2006).

10. Y.M. Chung, M.J. Jung, J.G. Han, M.W. Lee, and Y.M. Kim, *Thin Solid Films*. **447**, (2004).

11. S.I. Hong, K.B. Kim, Y. Lee, S.Y. Cho, J.A. Ko, S.K. Hong, and H.J. Park, *Journal of Applied Polymer Science*. **113**, 5, (2009).

12. J. Kowalonek, H. Kaczmarek, and A. Dabrowska, *Applied Surface Science*. **257**, 1, (2010).

13. H. Lim, Y. Lee, S. Han, Y. Kim, J.M. Song, and J.S. Kim, *Journal of Polymer Science Part B-Polymer Physics*. **41**, 15, (2003).

14. P. Pedrosa, J.M. Chappe, C. Fonseca, A.V. Machado, J.M. Nobrega, and F. Vaz, *Plasma Processes and Polymers*. **7**, 8, (2010).

15. K. Fricke, H. Steffen, T. von Woedtke, K. Schroder, and K.D. Weltmann, *Plasma Processes and Polymers*. **8**, 1, (2011).

16. S.R. Matthews, Y.J. Hwang, M.G. McCord, and M.A. Bourham, *Journal of Applied Polymer Science*. **94**, 6, (2004).

17. U. Little, F. Buchanan, E. Harkin-Jones, B. Graham, B. Fox, A. Boyd, B. Meenan, and G. Dickson, *Acta Biomaterialia*. **5**, 6, (2009).

18. J.M. Song, Y. Kim, S. Han, Y. Lee, and J.S. Kim, *Journal of Applied Polymer Science*. **89**, 11, (2003).

19. J. Kowalonek and K. Suchocka-Galas, *Applied Surface Science*. **255**, 22, (2009).

20. A.J. Ro, S.J. Huang, and R.A. Weiss, *Polymer*. **49**, 2, (2008).

21. S.G. Cho and K.C. Ko, *Current Applied Physics*. **11**, 3, (2011).

22. N. Encinas, M. Pantoja, J. Abenojar, and M.A. Martinez, *Journal of Adhesion Science and Technology*. **24**, 11-12, (2010).

23. M. Gindl, G. Sinn, W. Gindl, A. Reiterer, and S. Tschegg, *Colloids and Surfaces a-Physicochemical and Engineering Aspects*. **181**, 1-3, (2001).

24. Y. Uyama, H. Inoue, K. Ito, A. Kishida, and Y. Ikada, *Journal of Colloid and Interface Science*. **141**, 1, (1991).

25. T.A. Hill, D.L. Carroll, R. Czerw, C.W. Martin, and D. Perahia, *Journal of Polymer Science Part B-Polymer Physics*. **41**, 2, (2003).

26. R.S. McLean, M. Doyle, and B.B. Sauer, *Macromolecules*. **33**, 17, (2000).

27. B.B. Sauer and R.S. McLean, *Macromolecules*. **33**, 21, (2000).

28. Z.Q. Gao, *Applied Surface Science*. **257**, 7, (2011).

29. Z.Q. Gao, J. Sun, S.J. Peng, L. Yao, and Y.P. Qiu, *Journal of Applied Polymer Science*. **120**, 4, (2011).

30. I. Keranov, T.G. Vladkova, M. Minchev, A. Kostadinova, G. Altankov, and P. Dineff, *Journal of Applied Polymer Science*. **111**, 5, (2009).

31. K. Tsougeni, N. Vourdas, A. Tserepi, E. Gogolides, and C. Cardinaud, *Langmuir*. **25**, 19, (2009).

32. C.H. Zhang, P. Chen, B.L. Sun, W. Li, B.C. Wang, and J. Wang, *Applied Surface Science*. **254**, 18, (2008).

33. Z.I. Ali, *Journal of Applied Polymer Science*. **103**, 6, (2007).

34. R.M. Walters, K.E. Sohn, K.I. Winey, and R.J. Composto, *Journal of Polymer Science Part B-Polymer Physics*. **40**, 24, (2002).

Figure 1. Change in total surface energy (γ_S) of the sodium ionomer and its polar (γ_S^P) and dispersive (γ_S^d) components, as a function of velocity at a nozzle-substrate distance of 6mm.

Figure 2. Change in total surface energy (γ_S) of the sodium ionomer and its polar (γ_S^P) and dispersive (γ_S^d) components, as a function of velocity at a nozzle-substrate distance of 10mm.

Figure 3. Change in total surface energy (γ_S) of the sodium ionomer and its polar (γ_S^P) and dispersive (γ_S^d) components, as a function of velocity at a nozzle-substrate distance of 14mm.

Figure 4. Change in total surface energy (γ_S) of the sodium ionomer and its polar (γ_S^P) and dispersive (γ_S^d) components, as a function of velocity at a nozzle-substrate distance of 20mm.

Figure 5. AFM profiles for sodium ionomer samples, treated with plasma at a scan velocity of 100 mm/s for each nozzle-substrate distance. (a) untreated sample; (b) application distance of 6mm; (c) application distance of 10mm; (d) application distance of 14mm; (e) application distance of 20mm.

Figure 6. AFM profiles for sodium ionomer sample surfaces treated with atmospheric plasma at a nozzle-substrate distance of 6 mm as a function of scan velocity. Profile (a): untreated sample; Profile (b): sample treated at 100 mm·s^{-1}; Profile (c): sample treated at 300 mm·s^{-1}; Profile (d): sample treated at 700 mm·s^{-1}; Profile (e): sample treated at 1000 mm·s^{-1}.

Figure 7. AFM profiles for sodium ionomer sample surfaces treated with atmospheric plasma at a nozzle-substrate distance of 10 mm as a function of scan velocity. Profile (a): untreated sample; Profile (b): sample treated at 100 mm·s^{-1}; Profile (c): sample

treated at 300 mm·s^{-1}; Profile (d): sample treated at 700 mm·s^{-1}; Profile (e): sample treated at 1000 mm·s^{-1}.

Figure 8. AFM profiles for sodium ionomer sample surfaces treated with atmospheric plasma at a nozzle-substrate distance of 14 mm as a function of scan velocity. Profile (a): untreated sample; Profile (b): sample treated at 100 mm·s^{-1}; Profile (c): sample treated at 300 mm·s^{-1}; Profile (d): sample treated at 700 mm·s^{-1}; Profile (e): sample treated at 1000 mm·s^{-1}.

Figure 9. AFM profiles for sodium ionomer sample surfaces treated with atmospheric plasma at a nozzle-substrate distance of 20 mm as a function of scan velocity. Profile (a): untreated sample; Profile (b): sample treated at 100 mm·s^{-1}; Profile (c): sample treated at 300 mm·s^{-1}; Profile (d): sample treated at 700 mm·s^{-1}; Profile (e): sample treated at 1000 mm·s^{-1}.

Figure 10. FTIR-ATR graph showing sodium ionomers treated with atmospheric plasma at an application velocity of 100 mm/s as a function of various nozzle/substrate distances. (a) original ionomer, (b) ionomer treated at a distance of 6mm, (c) ionomer treated at a distance of 10mm, (d) ionomer treated at a distance of 14mm, (e) ionomer treated at a distance of 20mm.

Table 1. Characteristics of various contact liquids featuring different polarities which were used in measurement of contact angles to determine surface energy of ionomer films.

Contact Liquids	γ_l^d(mJ·m^{-2})	γ_l^p(mJ·m^{-2})	γ_l(mJ·m^{-2})
water	22.0	50.2	72.2
glycerol	34.0	30.0	64.0
diiodomethane	48.5	2.3	50.8
formamide	32.3	26.0	58.3

Table 2. Variation in contact angles on the sodium ionomer film surface, measured using different contact liquids as a function of scan velocity at a distance of 6 mm between nozzle and substrate.

Speed (mm/s)	WATER		FORMAMIDE		DIODOMETHANE		GLYCEROL	
	θ	σ	θ	σ	θ	σ	θ	σ
100	24,6	1,8	15,1	1,2	24,2	1,9	30,9	0,6
300	47,7	1,4	25,3	0,6	37,1	0,7	48,0	0,6
500	53,5	1,4	36,5	1,0	42,4	0,7	58,1	1,2
700	58,6	1,2	46,5	1,5	48,0	1,5	63,1	1,1
1000	63,8	1,2	52,2	1,0	50,3	1,8	66,6	0,2

Table 3. Variation in contact angles on the sodium ionomer film surface, measured using different contact liquids as a function of scan velocity at a distance of 10 mm between nozzle and substrate.

Speed (mm/s)	WATER		FORMAMIDE		DIODOMETHANE		GLYCEROL	
	θ	σ	θ	σ	θ	σ	θ	σ
100	43,1	1,5	33,1	0,3	38,9	0,7	40,8	0,7
300	52,0	0,9	41,0	0,6	41,4	0,3	47,8	0,6
500	59,6	1,1	46,2	0,7	45,9	1,0	53,3	0,4
700	63,7	1,0	49,8	0,5	49,1	0,9	61,5	0,5
1000	67,8	0,5	55,4	0,3	52,8	0,8	65,0	0,7

Table 4. Variation in contact angles on the sodium ionomer film surface, measured using different contact liquids as a function of scan velocity at a distance of 14 mm between nozzle and substrate.

Speed (mm/s)	WATER		FORMAMIDE		DIODOMETHANE		GLYCEROL	
	θ	σ	θ	σ	θ	σ	θ	σ
100	59,1	0,6	37,4	0,4	39,4	0,9	46,3	0,3
300	62,3	0,6	42,8	0,7	42,6	1,3	55,7	0,9
500	64,7	0,5	45,5	0,3	49,9	0,5	62,6	0,1
700	68,1	0,6	52,3	1,3	54,1	0,6	64,4	0,4
1000	70,8	0,5	55,1	0,1	55,9	0,5	66,0	0,3

Table 5. Variation in contact angles on the sodium ionomer film surface, measured using different contact liquids as a function of scan velocity at a distance of 20 mm between nozzle and substrate.

Speed (mm/s)	WATER		FORMAMIDE		DIODOMETHANE		GLYCEROL	
	θ	σ	θ	σ	θ	σ	θ	σ
100	60,1	0,8	43,9	1,4	35,8	0,3	56,1	0,4
300	65,5	0,9	52,8	1,0	40,2	0,9	62,3	0,1
500	68,3	1,1	58,4	0,4	46,1	0,5	64,6	0,2
700	71,6	1,0	58,7	0,1	51,6	0,3	66,7	0,1
1000	75,6	0,6	59,0	0,3	54,3	0,3	68,6	0,2

Table 6. Values for contact angles for an untreated sodium ionomer sample.

	WATER		FORMAMIDE		DIODOMETHANE		GLYCEROL	
	θ	σ	θ	σ	θ	σ	θ	σ
IO1.0	77,6	1,2	69,4	0,9	56,5	1,1	59,4	1,0

Table 7. Morphological parameters of sodium ionomer, determined using atomic force microscopy (AFM). Mean roughness (Rms) and Maximum roughness (Rmax).

D (mm)	0	6				10				14				20			
S (mm/s)	0	100	300	700	1000	100	300	700	1000	100	300	700	1000	100	300	700	1000
Rms (nm)	18.5	67.4	67.0	51.9	42.9	61.7	52.2	32.5	24.4	58.6	50.2	28.7	19.6	56.2	39.0	22.9	18.9
Rmax (nm)	281.7	411.0	396.6	485.2	418.6	395.3	310.6	282.6	233.3	436.5	473.8	455.1	469.8	385.7	341.1	218.4	533.3

Table 8. Measured values for area under peak at 1698.55 cm^{-1}, which corresponds to the methacrylic acid C=O group, in sodium ionomer samples treated at a velocity of 100 mm/s as a function of varying nozzle-substrate distances.

Line figure 10	Sample	Peek area 1698.55 cm^{-1}
(a)	Ionomer base	242.35 ua
(b)	6-100	343.09 ua
(c)	10-100	255.25 ua
(d)	14-100	253.75 ua
(e)	20-100	251.15 ua

Table 9. Values for area under peak at 1968.55 cm^{-1}, which corresponds to the methacrylic acid group C=O, as a function of plasma application velocity for samples treated at a nozzle-substrate distance of 6 mm.

Sample	Plasma treatment speed (mm/s)	Peek area 1698.55 cm^{-1} (ua)
Ionomer base	-	242.35
6-100	100	343.09
6-300	300	318.31
6-700	700	242.5
6-1000	1000	240.9

Table 10. Values for area under peak at 1968.55 cm^{-1}, which corresponds to the methacrylic acid group C=O, as a function of plasma application velocity for samples treated at a nozzle-substrate distance of 10 mm.

Sample	Plasma treatment speed (mm/s)	Peek area 1698.55 cm^{-1} (ua)
Ionomer base	-	242.35
10-100	100	255.25
10-300	300	249.19
10-700	700	247.91
10-1000	1000	245.87

Table 11. Values for area under peak at 1968.55 cm^{-1}, which corresponds to the methacrylic acid group C=O, as a function of plasma application velocity for samples treated at a nozzle-substrate distance of 14 mm.

Sample	Plasma treatment speed (mm/s)	Peek area 1698.55 cm^{-1} (ua)
Ionomer base	-	242.35
14-100	100	253.75
14-300	300	247.98
14-700	700	246.82
14-1000	1000	244.66

Table 12. Values for area under peak at 1968.55 cm^{-1}, which corresponds to the methacrylic acid group C=O, as a function of plasma application velocity for samples treated at a nozzle-substrate distance of 20 mm.

Sample	Plasma treatment speed (mm/s)	Peek area 1698.55 cm^{-1} (ua)
Ionomer base	-	242.35
20-100	100	251.15
20-300	300	248.98
20-700	700	246.64
20-1000	1000	243.84
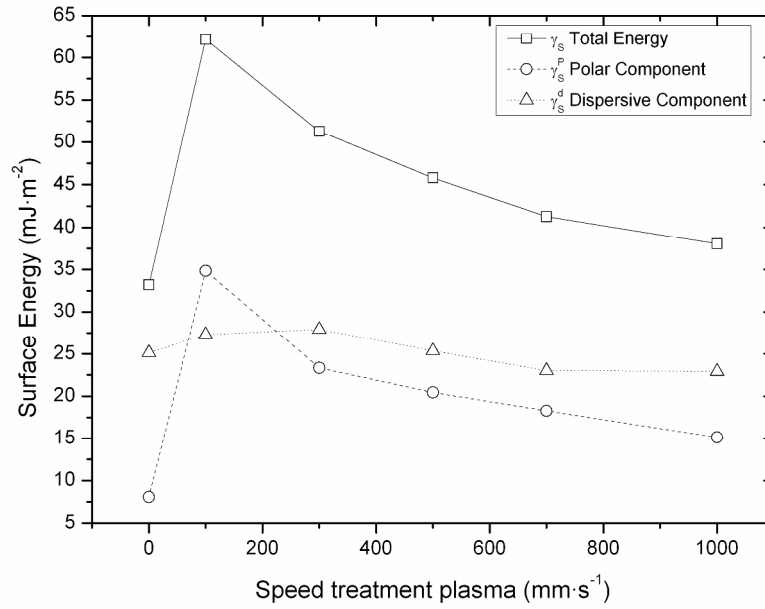
Figure 1. Change in total surface energy (γ_S) of the sodium ionomer and its polar (γ_S^P) and dispersive (γ_S^d) components, as a function of velocity at a nozzle-substrate distance of 6mm.
297x210mm (300 x 300 DPI)
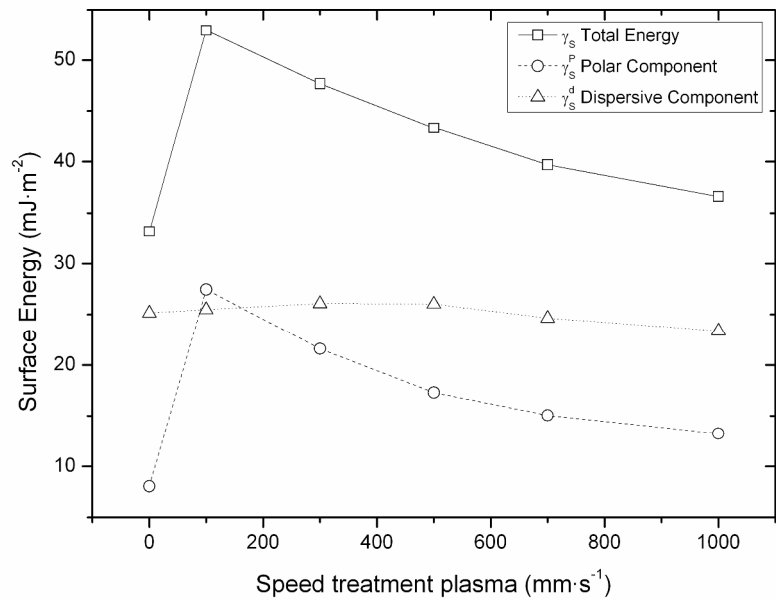
Figure 2. Change in total surface energy (γ_S) of the sodium ionomer and its polar (γ_S^P) and dispersive (γ_S^d) components, as a function of velocity at a nozzle-substrate distance of 10mm.
297x209mm (300 x 300 DPI)
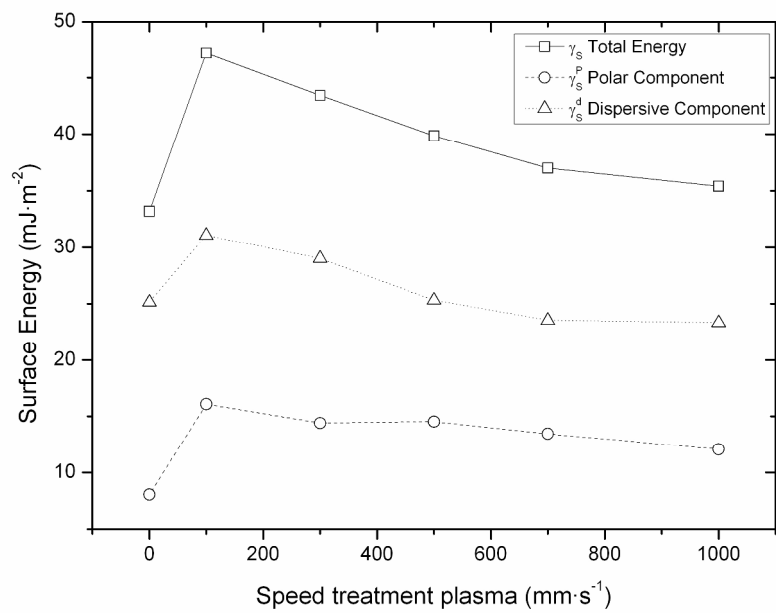
Figure 3. Change in total surface energy (γ_S) of the sodium ionomer and its polar (γ_S^P) and dispersive (γ_S^d) components, as a function of velocity at a nozzle-substrate distance of 14mm.
297x209mm (300 x 300 DPI)
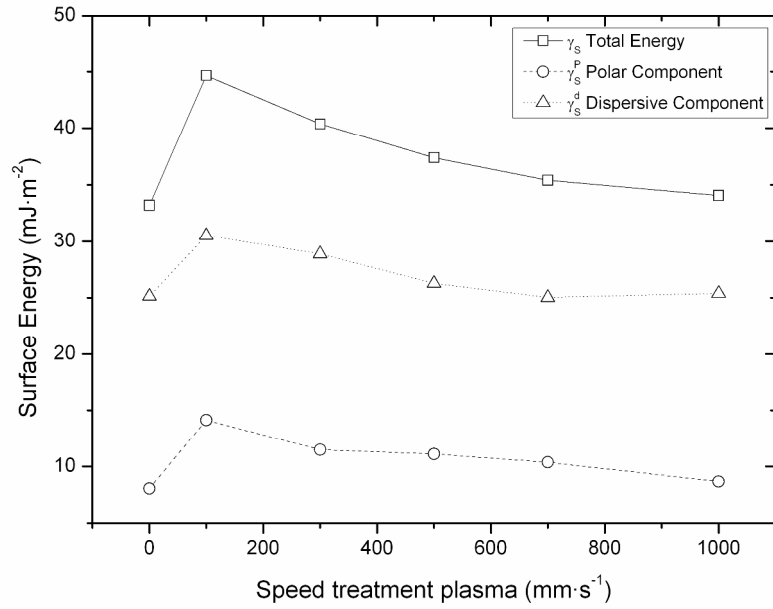
Figure 4. Change in total surface energy (γ_S) of the sodium ionomer and its polar (γ_S^P) and dispersive (γ_S^d) components, as a function of velocity at a nozzle-substrate distance of 20mm.
297x209mm (300 x 300 DPI)
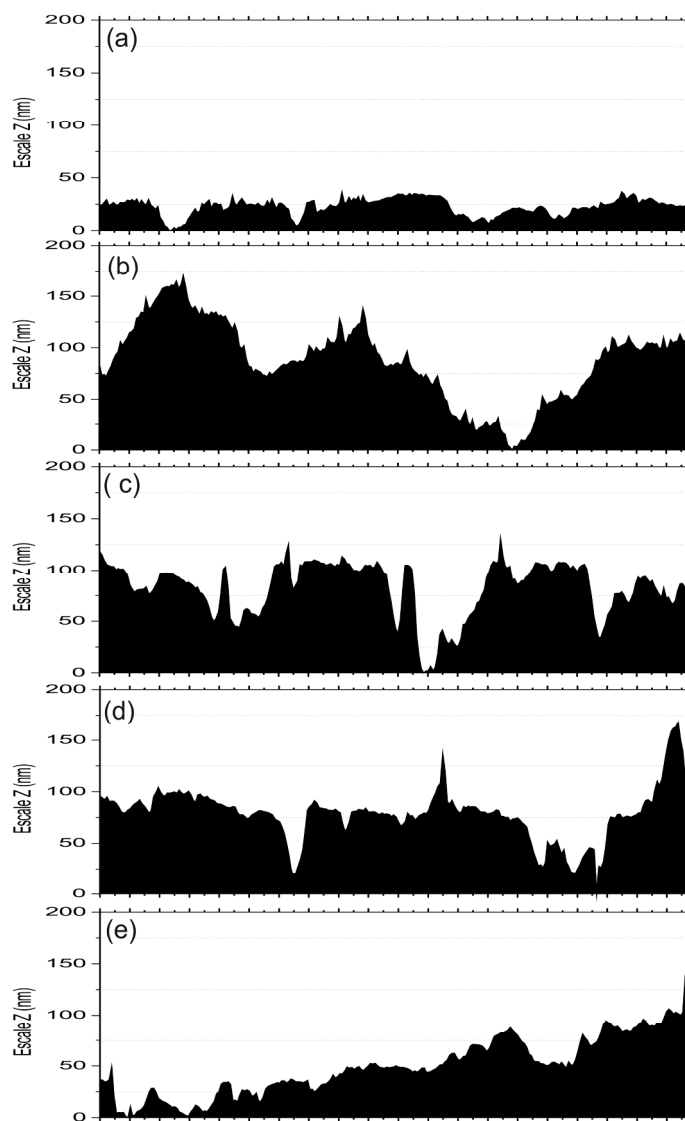
Figure 5. AFM profiles for sodium ionomer samples, treated with plasma at a scan velocity of 100 mm/s for each nozzle-substrate distance. (a) untreated sample; (b) application distance of 6mm; (c) application distance of 10mm; (d) application distance of 14mm; (e) application distance of 20mm. 150x263mm (300 x 300 DPI)
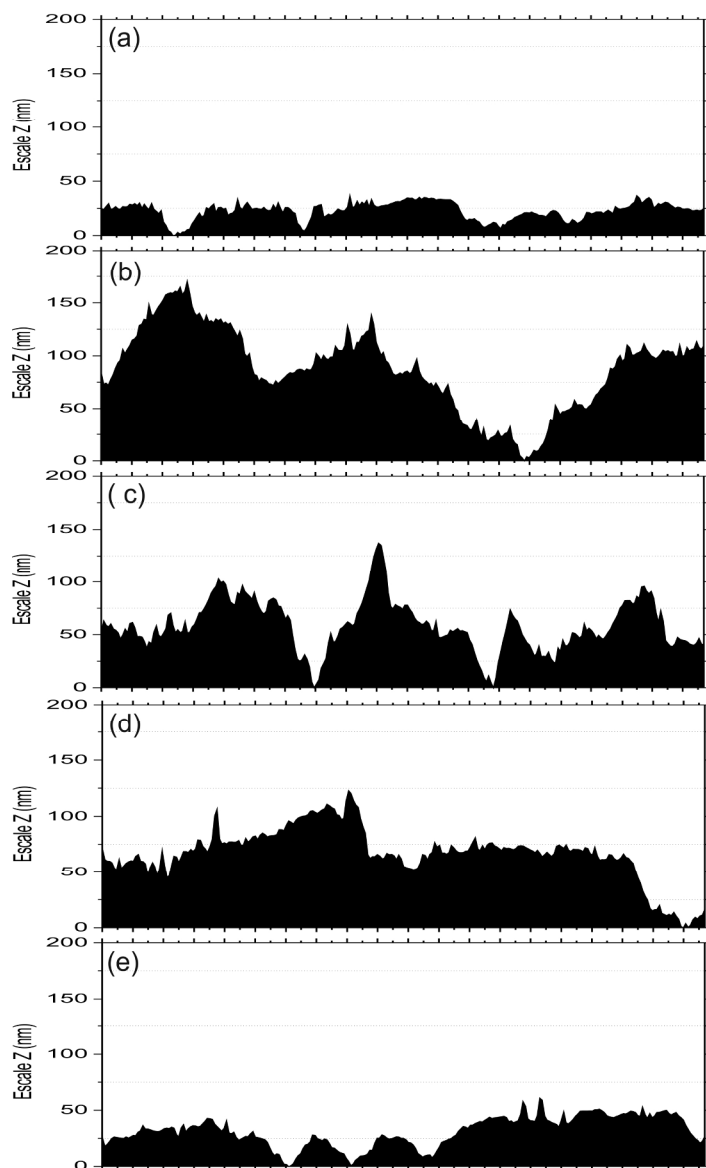
Figure 6. AFM profiles for sodium ionomer sample surfaces treated with atmospheric plasma at a nozzle-substrate distance of 6 mm as a function of scan velocity. Profile (a): untreated sample; Profile (b): sample treated at 100 mm·s^{-1}; Profile (c): sample treated at 300 mm·s^{-1}; Profile (d): sample treated at 700 mm·s^{-1}; Profile (e): sample treated at 1000 mm·s^{-1}.
150x256mm (300 x 300 DPI)
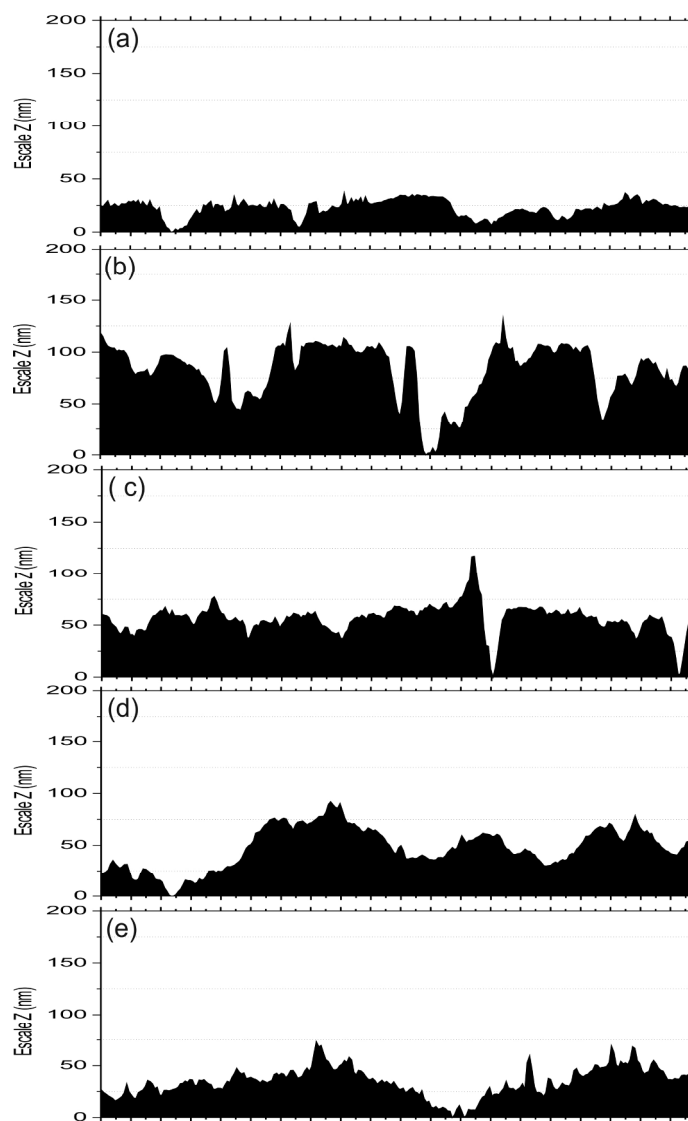
Figure 7. AFM profiles for sodium ionomer sample surfaces treated with atmospheric plasma at a nozzle-substrate distance of 10 mm as a function of scan velocity. Profile (a): untreated sample; Profile (b): sample treated at 100 mm·s^{-1}; Profile (c): sample treated at 300 mm·s^{-1}; Profile (d): sample treated at 700 mm·s^{-1}; Profile (e): sample treated at 1000 mm·s^{-1}.
150x262mm (300 x 300 DPI)
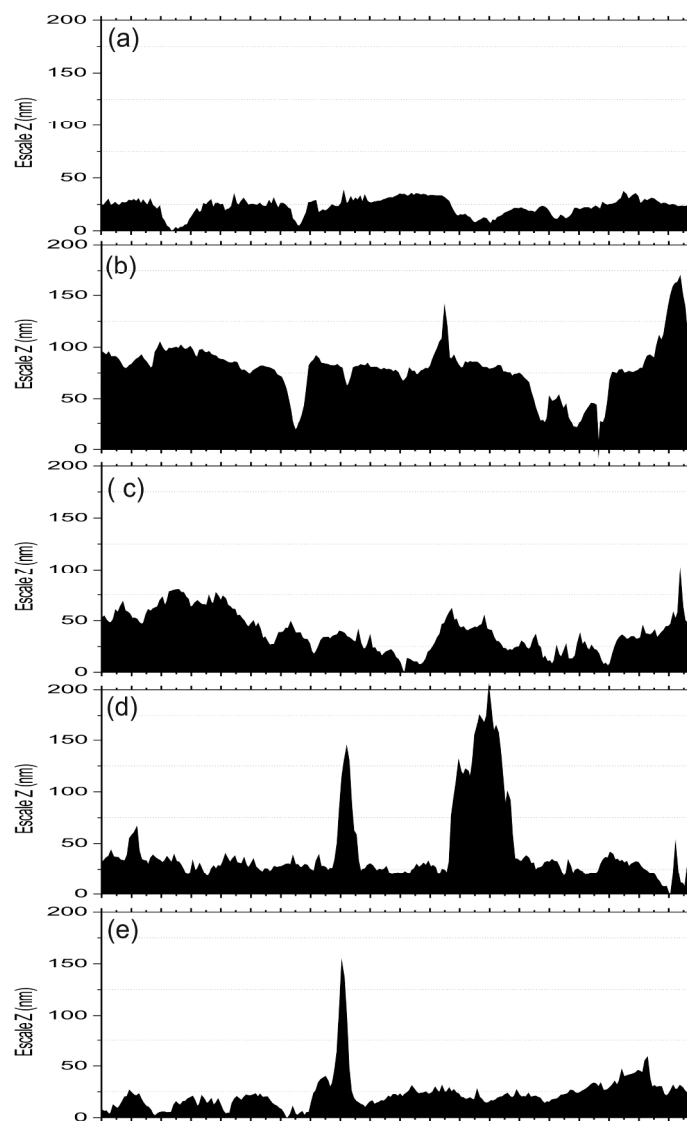
Figure 8. AFM profiles for sodium ionomer sample surfaces treated with atmospheric plasma at a nozzle-substrate distance of 14 mm as a function of scan velocity. Profile (a): untreated sample; Profile (b): sample treated at 100 mm·s^{-1}; Profile (c): sample treated at 300 mm·s^{-1}; Profile (d): sample treated at 700 mm·s^{-1}; Profile (e): sample treated at 1000 mm·s^{-1}.
150x263mm (300 x 300 DPI)
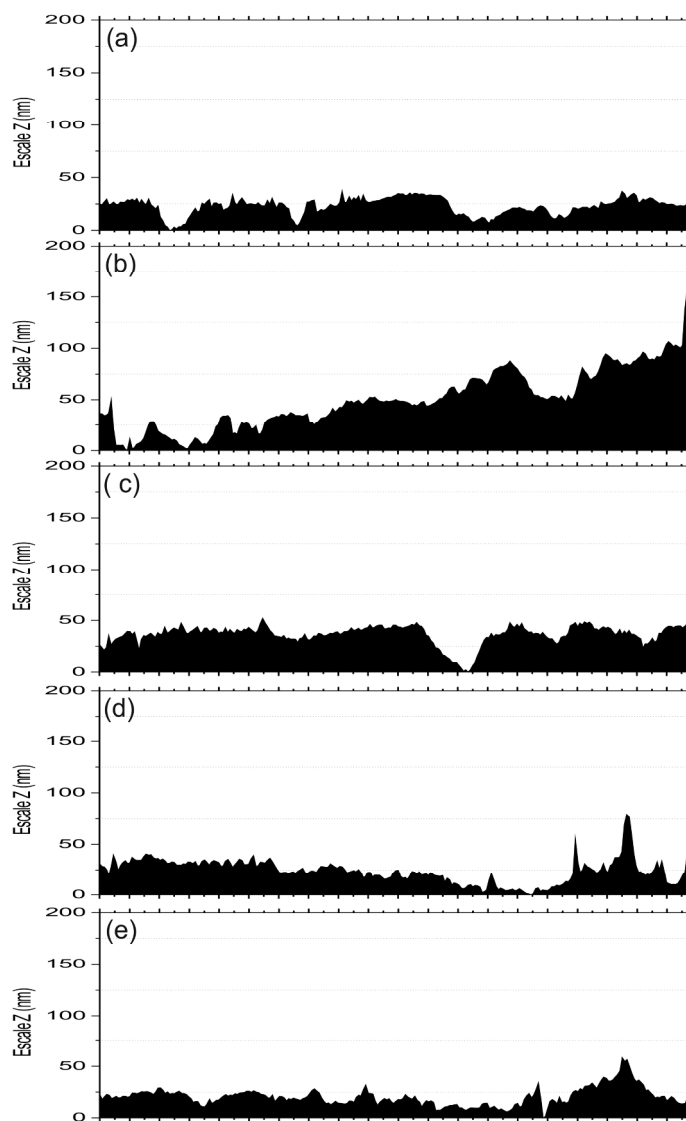
Figure 9. AFM profiles for sodium ionomer sample surfaces treated with atmospheric plasma at a nozzle-substrate distance of 20 mm as a function of scan velocity. Profile (a): untreated sample; Profile (b): sample treated at 100 mm·s^{-1}; Profile (c): sample treated at 300 mm·s^{-1}; Profile (d): sample treated at 700 mm·s^{-1}; Profile (e): sample treated at 1000 mm·s^{-1}.
150x264mm (300 x 300 DPI)
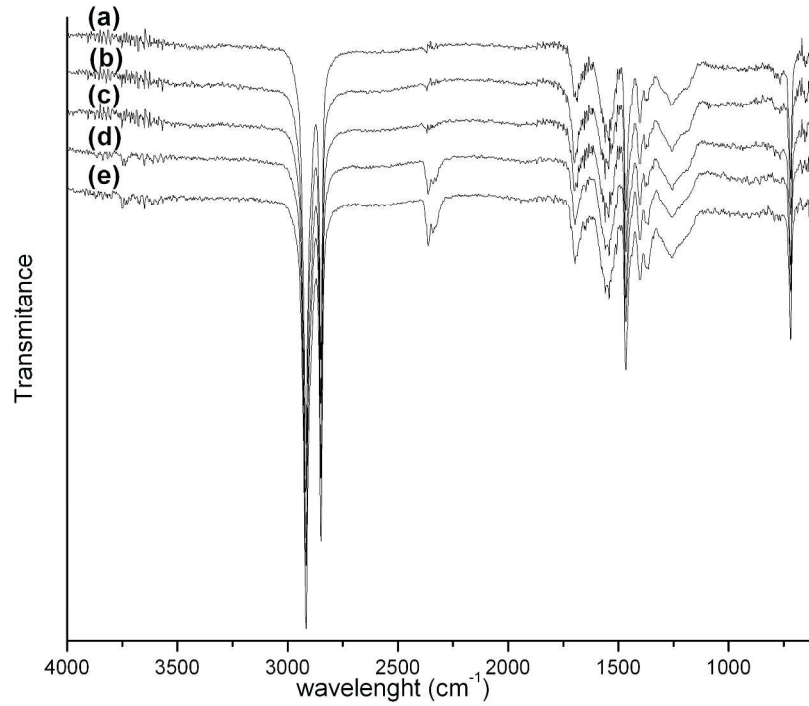
Figure 10. FTIR-ATR graph showing sodium ionomers treated with atmospheric plasma at an application velocity of 100 mm/s as a function of various nozzle/substrate distances. (a) original ionomer, (b) ionomer treated at a distance of 6mm, (c) ionomer treated at a distance of 10mm, (d) ionomer treated at a distance of 14mm, (e) ionomer treated at a distance of 20mm.
289x202mm (300 x 300 DPI)